Axial ligand effects on the diradical characters and second hyperpolarizabilities of open-shell singlet transition-metal dinuclear complexes

ARTICLE *in* CHEMICAL PHYSICS LETTERS · JULY 2014

Impact Factor: 1.9 · DOI: 10.1016/j.cplett.2014.05.064

5 AUTHORS, INCLUDING:

Benoît Champagne
University of Namur
401 PUBLICATIONS **8,733** CITATIONS
SEE PROFILE

Masayoshi Nakano
Osaka University
337 PUBLICATIONS **4,781** CITATIONS
SEE PROFILE

Chemical Physics Letters 608 (2014) 68–73

Contents lists available at ScienceDirect

Chemical Physics Letters

journal homepage: www.elsevier.com/locate/cplett

Editor's Choice

Axial ligand effects on the diradical characters and second hyperpolarizabilities of open-shell singlet transition-metal dinuclear complexes

Taishi Yamada [a], Shota Takamuku [a], Hiroshi Matsui [a], Benoît Champagne [b], Masayoshi Nakano [a,*]

[a] Department of Materials Engineering Science, Graduate School of Engineering Science, Osaka University, Toyonaka, Osaka 560-8531, Japan
[b] Laboratoire de Chimie Théorique, University of Namur, rue de Bruxelles, 61, B-5000 Namur, Belgium

ARTICLE INFO

Article history:
Received 23 April 2014
In final form 21 May 2014
Available online 2 June 2014

ABSTRACT

We investigate the axial ligand effects on the diradical character (y) dependences of the second hyperpolarizabilities (γ) of transition-metal dinuclear complexes, $Mo(I)_2(CO)_2$, with different bond lengths (R) using the spin-unrestricted coupled-cluster method. $Mo(I)_2(CO)_2$ exhibits intrinsic y–γ correlation and dominant dσ-electron contribution to the maximum γ (γ_{max}), which are also observed in the bare dinuclear analogs. The axial-ligand coordination to $Mo(I)_2$ is found to cause the increase of the diradical character of the dσ orbital, the emergence of large negative γ for small R, and an enhancement of $|\gamma_{max}|$ by a factor of ~30 as compared to the bare analogs.

1. Introduction

Recently, open-shell singlet molecules have attracted much attention among theoretical and experimental researchers in both chemistry and physics due to their unique electronic, magnetic and optical functions [1–4]. Among their unique functions, theoretical investigations have shown that they display a strong correlation between the open-shell character and the nonlinear optical (NLO) properties (hereafter referred to as 'y–γ correlation'), which states that singlet diradical systems with an intermediate diradical character exhibit larger second hyperpolarizabilities γ (the third-order NLO properties at the molecular scale) than pure diradical and closed-shell systems of similar size [5,6]. This theoretical principle has been experimentally confirmed by two-photon absorption [7,8] and third-harmonic generation [9,10] measurements.

On the basis of this principle, we have theoretically investigated several realistic open-shell singlet molecular systems exhibiting large γ values [11,12]. Among them, transition-metal dinuclear complexes with weak metal–metal multiple bonds, exhibit a strong y–γ correlation [13–15]. Homo- and hetero-dinuclear transition metal systems without ligands (bare systems) are 'σ-dominant' third-order NLO systems [13,14], because the weak σ-bonds with intermediate diradical character primarily contribute to their γ values. Moreover, in these multiply-bonded systems, the γ amplitudes can be controlled by adjusting the metal–metal bond length, the metal elements, and their relative electronegativities [14,15]. On the other hand, most transition-metal compounds exist as complexes including ligands, and the charge transfer between metal (M) and ligand (L) is known to have impact on the NLO responses [16–18]. To extend the range of validity of the y–γ design guidelines, it is therefore appealing to study the ligand effects in realistic metal complexes. The ligand coordination can be equatorial or axial [19]. Recently, equatorial coordination has been studied in $Re_2(IV)F_8$ [20], demonstrating this compound exhibits the y–γ correlation and belongs to the 'σ-dominant' third-order NLO systems like the corresponding bare systems [13–15]. In addition, for a given metal–metal bond length, $Re(IV)_2F_8$ presents a smaller diradical character $y(dX)$ ($X = \sigma$ and π) than $Re(IV)_2$, which originates from the increase of the orbital energy gap as well as from the decrease of the exchange integrals between X-bonding and -anti-bonding orbitals owing to the equatorial F^- ligands. Thus, the equatorial ligand effects cause the elongation of the bond length leading to intermediate y values, resulting in the enhancement of the maximum γ by a factor of ~8 as compared to the bare $Re(IV)_2$ system [20]. Axial ligand effects are expected to be even more significant than the equatorial ones due to the coordination along the axis of the metal–metal bond, which is the origin of the open-shell nature. In this study, we examine the axial ligand effects on y and γ of M_2L_2 complexes composed of two M–L units (M = Mo(I), L = CO) in comparison with those of the corresponding bare dinuclear system, $Mo(I)_2$. Both systems possess a formally quintuple metal–metal bond composed of one dσ, two equivalent dπ and dδ bonds, and are expected to generate prototypical models

* Corresponding author. Fax: +81 6 6850 6268.
E-mail address: mnaka@cheng.es.osaka-u.ac.jp (M. Nakano).

http://dx.doi.org/10.1016/j.cplett.2014.05.064
0009-2614/

with a wide range of diradical characters by varying the metal–metal bond length as observed in our previous studies [20]. These results aim at extending the range of applicability of the y–γ correlation to metal–metal multiply-bonded complexes coordinated by axial ligands, as well as at constructing novel design guidelines for achieving remarkable NLO responses.

2. Model systems and calculation methods

Figure 1 shows the $Mo(I)_2(CO)_2$ model complex with $D_{\infty h}$ symmetry. Although there are many metal complexes coordinated with axial ligands, e.g., halogen (F^- and Cl^-), THF (tetrahydrofuran), Cp (ferrocene), NH_3, and CO, metal complexes only stabilized by axial ligands are not known yet [19]. However, we here examine a model complex coordinated with typical axial ligands, CO. $Mo(I)_2$ with and without CO ligands possesses five formal bond order (FBO) and bears one dσ bond and two equivalent dπ and dδ bonds resulting from the d^5–d^5 interaction. The present results can be compared with those of homo- and hetero-dinuclear models of group 6 metals including Mo [13–15]. In order to clarify the bond length dependences of the diradical characters as well as of the longitudinal γ values along the bond (z) axis, the Mo–Mo bond length (R) was varied from 1.6 to 4.4 Å, which leads to a wide range of diradical characters ($0 < y < 1$). In this regard, the other geometrical parameters are fixed to those of the equilibrium structure of $Mo(I)_2(CO)_2$ optimized at the RB3LYP level of approximation under the constraint of $D_{\infty h}$ symmetry (see Figure 1).

In all calculations, we employed (i) for the Mo atoms the effective core potential (ECP) of the Stuttgart group, which includes relativistic effects, with the corresponding valence basis set (SDD) [21], and (ii) for the for C and O atoms the 6-311+G* basis set. The SDD basis set was however supplemented with an additional set of f polarization functions ($\zeta_f = 1.0430$) (referred to as 'SDD(f)' in this study) [22]. As previously found for closed-shell [23] and open-shell singlet systems [24,25], extended basis sets (with diffuse functions) are indispensable for obtaining quantitative γ values. Note that the SDD basis set already includes one set of diffuse s, two sets of diffuse p, and one set of diffuse d functions. The 6-311+G* basis set used for the ligand atoms includes one set of diffuse p functions. These basis sets should be sufficient for describing the primary ligand effects on the y and on the γ values of transition metal–metal bonded complexes at the spin-unrestricted (U) coupled-cluster level with singles and doubles (UCCSD) and that with the perturbative triples [UCCSD(T)] [13–15], though more detailed analysis on the method and basis set sensitivity of the y and γ values for such systems will be an interesting theme in the future work.

The diradical character y can be approximately defined using the spin-projected occupation number of the spin-unrestricted Hartree–Fock natural orbital (UNOs) [26]:

$$y_i = 1 - \frac{2T_i}{1+T_i^2}, \quad \text{where} \quad T_i = \frac{n_{\mathrm{HONO}-i} - n_{\mathrm{LUNO}+i}}{2}. \tag{1}$$

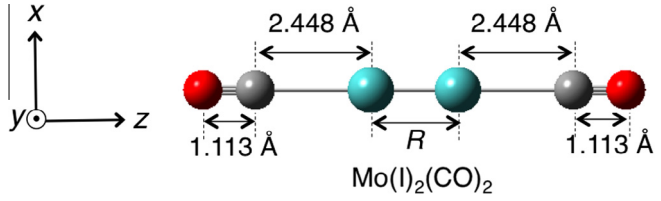

Figure 1. Structure of $Mo(I)_2(CO)_2$, where red, gray and blue balls represent C, O and Mo atoms, respectively. The metal–metal bond length R [Å] is varied from 1.6 to 4.4 Å with fixed Mo–C (2.448 Å) and C–O bond lengths (1.113 Å). These fixed bond lengths are obtained from the RB3LYP-optimized equilibrium structure of $Mo(I)_2(CO)_2$, where Mo–Mo bond length is 1.848 Å. Coordinate axes are also shown.

Here, $n_{\mathrm{HONO}-i}$ and $n_{\mathrm{LUNO}+i}$ represent the occupation numbers of the highest occupied natural orbitals HONO−i and the lowest unoccupied natural orbitals LUNO+i (where $i = 0, 1, \ldots$), respectively. y_i ranges from 0 to 1, which represents closed-shell and pure diradical states, respectively. In this study, the diradical characters are evaluated for the different dX orbitals [y(dX), where $X = \sigma$, π and δ] from the occupation numbers of the corresponding dX bonding and anti-bonding NO pairs. This method was shown to well reproduce the diradical characters of transition metal–metal bonded systems by other methods such as complete active space SCF and UCCSD methods [13].

The static bond-axis component γ_{zzzz} (simply referred to as γ, hereafter) values were calculated at the UCCSD and UCCSD(T) level of approximation using the finite-field (FF) approach [27], which consists in a forth-order differentiation of the energy with respect to the applied electric field. The power series expansion (called B convention [28]) was chosen for defining γ. A tight convergence threshold of 10^{-10} a.u. was used on the energy to obtain precise γ values. At the UCCSD level, γ was then partitioned into the contributions of the dX electrons [γ(dX)], calculated from the corresponding γ(dX) density [$d^{\mathrm{d}X(3)}(\mathbf{r})$] [29,30]:

$$\gamma(\mathrm{d}X) = \frac{1}{3!}\int z d^{\mathrm{d}X(3)}(\mathbf{r}) d\mathbf{r}, \tag{2}$$

where [$d^{\mathrm{d}X(3)}(\mathbf{r})$] is the third-order electric field derivative of the electron density, referred to as γ(dX) density [30], of the bonding (dX) and anti-bonding (dX^*) NO pair and it reads

$$d^{\mathrm{d}X(3)}(\mathbf{r}) = \frac{\partial}{\partial F^3}\{n_{\mathrm{d}X}\phi^*_{\mathrm{d}X}(\mathbf{r})\phi_{\mathrm{d}X}(\mathbf{r}) + n_{\mathrm{d}X^*}\phi^*_{\mathrm{d}X^*}(\mathbf{r})\phi_{\mathrm{d}X^*}(\mathbf{r})\}\Big|_{F=0}. \tag{3}$$

Here, $\phi_{\mathrm{d}X}(\mathbf{r})$ and $n_{\mathrm{d}X}$ represent the dX NO and its occupation number, respectively. Time-dependent(TD)-UB3LYP calculations were also performed to evaluate the excitation energies and transition moments with the SDD(f) basis set for the Mo atoms and the 6-311+G* basis set for the ligand atoms. All these calculations were performed using the GAUSSIAN 09 program package [31].

3. Results and discussion

3.1. Axial ligand effect on the diradical characters

Figure 2 shows the bond length (R) dependences of y(dX) ($X = \sigma$, π, and δ) for $Mo(I)_2$ and $Mo(I)_2(CO)_2$ systems. In both systems, all y(dX) values increase with R due to decreasing the d–d orbital over-

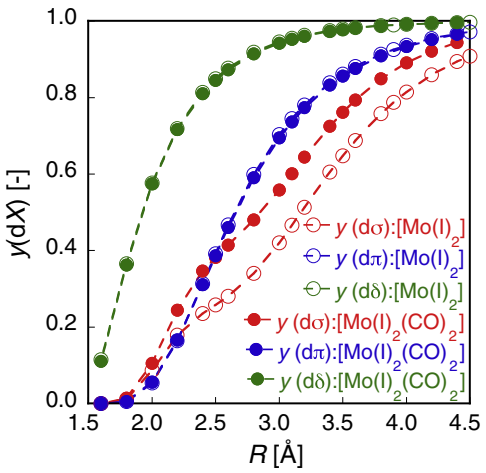

Figure 2. Evolution of the diradical characters [y(dX), $X = \sigma$, π and δ] as a function of the metal–metal bond length (R) in $Mo(I)_2$ and $Mo(I)_2(CO)_2$ obtained using the PUHF method.

laps while their amplitude ordering follows the relation $y(d\delta) > y(d\pi) > y(d\sigma)$ for any $R > \sim 2.2$ Å and $R > \sim 2.4$ Å in $Mo(I)_2$ and $Mo(I)_2(CO)_2$, respectively. This ordering reflects the amplitude of the dδ–dδ, dπ–dπ and dσ–dσ overlaps. At small R values, $y(d\pi) < y(d\sigma)$, which is attributed to the dz^2 anti-phase ring effect [14]. Unlike for the equatorial ligands, for any R, $y(d\sigma)$ of $Mo(I)_2(CO)_2$ is larger than that of $Mo(I)_2$, while their $y(d\pi)$ and $y(d\delta)$ values almost coincide.

In order to clarify the origin of the increase in $y(d\sigma)$ due to the axial ligand coordination, we examine the M–L interactions between five 4d orbitals of Mo and the valence σ and π orbitals of CO at the Hartree–Fock (HF) level of approximation (Figure 3a). It is found that the d_{yz} and d_{zx} (π symmetry) orbitals interact with the CO π orbitals [(HOMO−1, HOMO−2) of CO], and make bonding (1π, 1π) (with larger distributions on CO) and anti-bonding (2π, 2π′) (with larger distributions on Mo) orbitals, while the d_{xy} and $d_{x^2-y^2}$ (δ symmetry) orbitals do not interact with any valence orbitals of CO and thus form two non-bonding orbitals (1δ, 1δ). Furthermore, the $4d_{z^2}$ (σ symmetry) orbital interacts with the CO σ orbital (HOMO of CO), to create bonding (1σ) (with larger distributions on CO) and anti-bonding (2σ) (with larger distributions on Mo $4d_{z^2}$) orbitals. Due to symmetry, the Mo 5s orbital (with higher energy than that of $4d_{z^2}$) is also expected to interact with the 2σ orbital of Mo–CO, resulting in a slight stabilization of the anti-bonding 2σ orbital. Indeed, it is found from spin-unrestricted HF (UHF) calculations that the out-of-phase combination of the 5s and $4d_{z^2}$ orbitals (see Figure 3a) leads to the relative enhancement

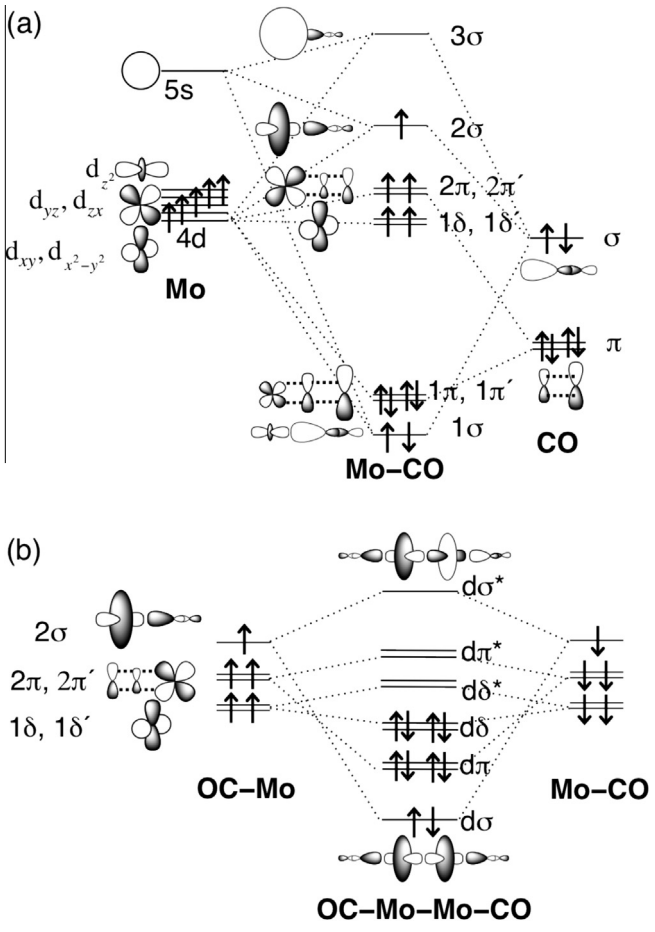

Figure 3. Schematic orbital correlation diagrams between Mo(I) and CO (a) and between two Mo(I)–CO units (b) at the Hartree–Fock level of approximation. (a) shows the correlation between the valence orbitals of the Mo(I) sextet and of the singlet CO, which generates the Mo(I)–CO sextet, while (b) shows the correlation between these two sextets leading to the $Mo(I)_2(CO)_2$ singlet. For the two degenerate orbitals with π and δ symmetry, one orbital diagram is only sketched.

of the ring component of $4d_{z^2}$ orbital as well as to the relative reduction of the bond-axis component of $4d_{z^2}$, which is referred to as the out-of-phase 'sd_{z^2} hybridization' hereafter. This hybridization attenuates therefore the anti-bonding nature between the bond-axis component of $4d_{z^2}$ of Mo and the σ lobe of CO, while it increases the bonding nature between anti-phase ring of $4d_{z^2}$ of Mo and σ lobe of CO (see 2σ orbital in Figure 3a). Moreover, the in-phase sd_{z^2} hybridization stabilizes the 1σ energy and the anti-phase mixing between 5s of Mo and σ of CO makes the anti-bonding 3σ orbital (with larger distributions on Mo 5s). In general, such hybridization of the 5s and 4d orbitals is observed in heavy transition-metal complexes where it induces stabilization of the occupied orbitals [32]. In the present case, the occupied 1σ and 2σ (unoccupied 3σ) are stabilized (destabilized) by such hybridization. As a result, the 2σ, 2π, 2π′, 1δ and 1δ′ orbitals are primarily distributed on Mo, i.e., five split 4d-based orbitals are formed, and they interact with those of the second Mo–CO unit, leading to d^5–d^5 interaction (see Figure 3b). Since the diradical character primarily contributing to γ is associated with the dσ orbital, we now focus on the interaction between the 2σ orbitals of the two Mo–CO moieties, which form the Mo–Mo dσ orbitals. We speculate that the shrinking of the bond-axis component of d_{z^2} in the 2σ orbital of Mo–CO causes the decrease of 2σ–2σ overlap, which increases $y(d\sigma)$.

In order to confirm this speculation, we examine the dσ natural orbital (NO) distributions and $y(d\sigma)$ of $Mo(I)_2$ and $Mo(I)_2(CO)_2$ at several R' (Mo–CO bond lengths) [$R' = 1.8$, 2.0, 2.448 (optimized distance), and 3.0 Å] while keeping $R = 3.5$ Å, where $Mo(I)_2(CO)_2$ has a maximum γ value for $R' = 2.448$ Å (see Figure 4). When R' decreases, the ring components of the d_{z^2} NO distributions increase and the component along bond axis is reduced, and therefore $y(d\sigma)$ increases as the CO approaches the metal. These results substantiate our speculation: $y(d\sigma)$ increases due to the out-of-phase sd_{z^2} hybridization caused by the coordination of axial CO ligands. On the other hand, equatorial ligands give rise to in-phase sd_{z^2} hybridization in dσ orbital that enlarges the bond-axis component of the dσ orbital, which decreases $y(d\sigma)$ [20]. Therefore, the opposite effects on the diradical characters of the equatorial and axial coordinations originate from the in- and out-of-phase sd_{z^2} hybridizations in the dσ orbital.

3.2. Axial ligand effect on the γ values

Figure 5a and b show the R-dependences of γ and of $\gamma(dX)$ for the bare [$Mo(I)_2$] and complex [$Mo(I)_2(CO)_2$] systems, respectively. The UCCSD method is found to closely reproduce the UCCSD(T) γ values of both systems, demonstrating the small contribution of the perturbative triple excitations and allowing to use the UCCSD method to analyze γ in terms of its contributions. For $Mo(I)_2$, γ is positive, is dominated by $\gamma(d\sigma)$, and is maximized in the intermediate y region [$\gamma_{max} = 4.76 \times 10^4$ a.u. for $y(d\sigma)_{max} = 0.788$ at $R_{max} = 3.9$ Å]. On the other hand, for $Mo(I)_2(CO)_2$, γ presents two extrema, one positive [$\gamma_{max+} = 144 \times 10^4$ a.u. for $y(d\sigma)_{max+} = 0.761$ at $R_{max+} = 3.5$ Å], and one negative [$\gamma_{max-} = -155 \times 10^4$ a.u. for $y(d\sigma)_{max-} = 0.601$ at $R_{max-} = 3.1$ Å]. Again, $\gamma(d\sigma)$ is the primary contribution to γ. The axial ligands have therefore a double effect (i) an extremum with negative γ values of large amplitude appears at small R (<∼3.3 Å) in addition to the positive one, and (ii) both extrema correspond to γ amplitudes ($|\gamma_{max+}|$ and $|\gamma_{max-}|$) about 30 times as large as γ_{max} of $Mo(I)_2$.

To investigate the origin of the negative extremum, the perturbation theory expression of γ is adopted. For a symmetric system in the three-state approximation, it reads as [33].

$$\gamma = -4\frac{\mu_{n0}^4}{E_{n0}^3} + 4\frac{\mu_{n0}^2\mu_{nm}^2}{E_{n0}^2 E_{m0}}, \qquad (4)$$

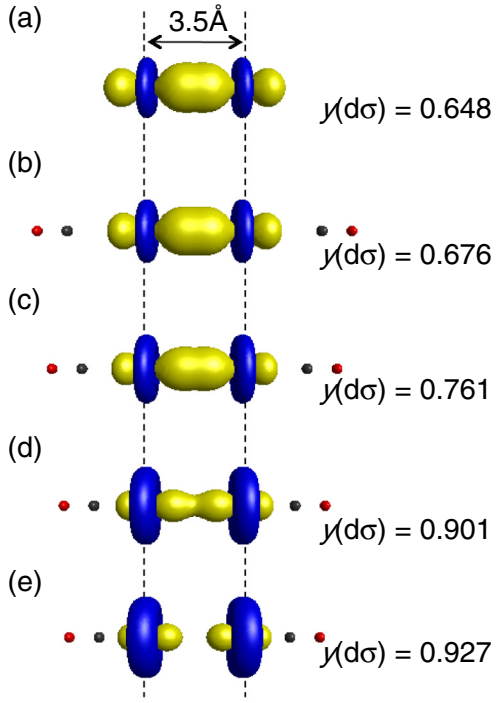

Figure 4. dσ natural orbitals and $y(d\sigma)$ of $Mo(I)_2$ (a) and $Mo(I)_2(CO)_2$ at R(Mo–CO) = 3.0 Å (b), 2.448 Å (c), 2.0 Å (d), 1.8 Å (e), for a metal–metal distance R(Mo–Mo) = 3.5 Å.

where μ_{ij} and E_{i0} represent the transition moment between states i and j (where 0 indicates the ground state), and the excitation energy of the ith excited state, respectively. On the right-hand side of Eq. (4), the first and second terms represent the contributions of type II (γ_{II}) and type III-2 ($\gamma_{III\text{-}2}$) virtual excitation processes, respectively [33]. Obviously, since $\gamma_{III\text{-}2}$ is positive, the negative γ value in the small R region originates from γ_{II}. Morever, within the same scheme, the polarizability α is expressed by

$$\alpha = 2\frac{\mu_{n0}^2}{E_{n0}}, \tag{5}$$

and therefore, γ_{II} can be rewritten as [33]

$$\gamma_{II} = -\frac{\alpha^2}{E_{n0}} = -\frac{\alpha^3}{2\,\mu_{n0}^2}. \tag{6}$$

The use of this simplified expression to analyze γ_{II} and γ is substantiated by the fact that the UCCSD α of $Mo(I)_2(CO)_2$ displays a maximum for the R value corresponding to the negative extremum of γ (Figure 6). α displays a bell-shape R dependence with a maximum at R_{max} (=3.1 Å) for $Mo(I)_2(CO)_2$ (α_{max} = 332 a.u.), which is about four times as large as that of $Mo(I)_2$ (α_{max} = 86.1 a.u. at R_{max} = 3.2 Å). This enhancement of α implies a decrease of the excitation energy E_{n0} and/or an increase of the transition moment amplitude μ_{n0} upon ligand coordination [see Eq. (5)]. Indeed, TD-UB3LYP calculations give (1.29 eV, 1.06 D) and (0.504 eV, 2.68 D) for (E_{n0}, $|\mu_{n0}|$) of $Mo(I)_2$ and $Mo(I)_2(CO)_2$ at R = 3.2 Å, respectively, which qualitatively supports their relative α_{max} amplitudes though the $\alpha_{max}(Mo(I)_2)/\alpha_{max}(Mo(I)_2(CO)_2$ (~17) ratio obtained by Eq. (5) using these results is larger than the FF result (~3.9), which is attributed to the lack of the other excited states contributions. Moreover, almost the same peak position (R = 3.1 Å) between α_{max} and γ_{max-} for $Mo(I)_2(CO)_2$ indicates that $\gamma^{III\text{-}2}$ is much smaller than γ^{II} around that distance because the maximum $\gamma^{III\text{-}2}$ is predicted to appear at a larger R value than the maximum $|\gamma^{II\text{-}1}|$ [6]. As a consequence, $|\gamma_{II}|$ increases in proportion to the cube of α [see Eq. (6)], which explains qualitatively the remarkable enhancement of the γ_{max-} amplitudes for $Mo(I)_2(CO)_2$ (155×10^4 a.u.) with respect to $Mo(I)_2$ (0.687×10^4 a.u.) at R = 3.1 Å.

Next, we analyze the significant enhancement of the positive extremum (γ_{max+}) due to the ligand coordination. R_{max+} of $Mo(I)_2(CO)_2$ is 0.4 Å smaller than that of $Mo(I)_2$ (Table 1), which is attributed to the increase, for a given R value, of $y(d\sigma)_{max+}$ due to the out-of-phase sd_{z^2} hybridization as described in the previous section. The origin of the 30 enhancement factor of γ_{max+} of $Mo(I)_2(CO)_2$ as compared to that of $Mo(I)_2$ can be explained as follows. As seen from the analytical formula of γ [Eq. (11) in Ref. [6]], γ is proportional to R^4/U^3, where U and R indicate the effective Coulomb repulsion and effective diradical distance in the localized NO (LNO) representation. U_{dX} is expressed by $2K_{dX}$, where K_{dX} represents the exchange integral between the symmetry-adapted bonding and anti-bonding dX orbitals (X = σ, π, and δ) [20]. We assume that the dominant contribution to γ_{max+} originates from the metal–metal bond and that only the variations in R_{max+} and $U_{d\sigma}$ lead to the significant enhancement of $\gamma(d\sigma)_{max+}$ for given $y(d\sigma)_{max+}$ values in $Mo(I)_2$ and $Mo(I)_2(CO)_2$. The $K_{d\sigma}$ values in $Mo(I)_2$ at R = 3.9 Å and $Mo(I)_2(CO)_2$ at R = 3.5 Å were evaluated from the excitation energies calculated at the complete active space CI(2,2) level of approximation using spin-unrestricted NOs (UNOs) (see Supplementary data of Ref. [20] for the calculation procedure). Under this assumption, the ratio $\gamma_{max}[Mo(I)_2(CO)_2]/\gamma_{max}[Mo(I)_2]$ is predicted to amount to $(R_{max+}[Mo(I)_2(CO)_2]/R_{max+}[Mo(I)_2])^4/(U_{d\sigma}[Mo(I)_2(CO)_2]/U_{d\sigma}[Mo(I)_2])^3 = (3.5/3.9)^4/(0.331/0.367)^3$ ~0.88, which cannot explain the significant enhancement ratio. This failure is attributed to the lack of dynamical electron correlation in calculating $U_{d\sigma}$ using the UNOCASCI(2,2) method and to the fact that these dynamical electron correlation effects

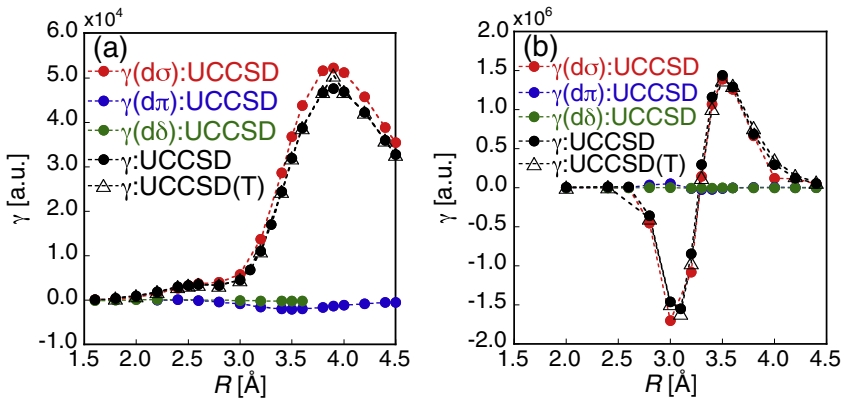

Figure 5. Evolution of γ as well as of its dX contributions [$\gamma(dX)$, X = σ, π, and δ] as a function of the metal–metal bond length (R) for $Mo(I)_2$ (a) and $Mo(I)_2(CO)_2$ (b) calculated using the UCCSD method.

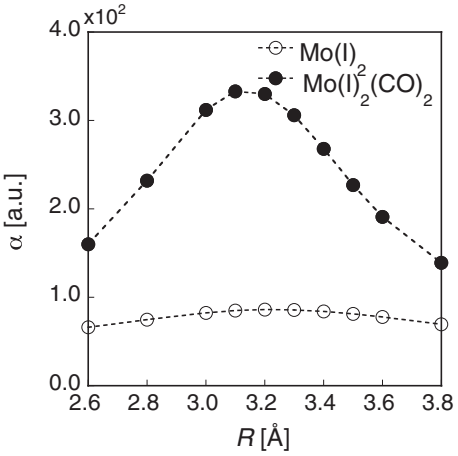

Figure 6. Evolution of α as a function of the metal–metal bond length (R) for $Mo(I)_2$ and $Mo(I)_2(CO)_2$ calculated using the UCCSD method.

Table 1
Characteristics of the γ positive extremum: maximum γ value (γ_{max+}), dσ contribution to γ_{max+} [$\gamma_{max+}(d\sigma)$] as well as corresponding bond lengths (R_{max+}) and diradical characters [$y(d\sigma)_{max+}$] for $Mo(I)_2$ and $Mo(I)_2(CO)_2$.

	γ_{max+} [$\times 10^4$ a.u.]	$\gamma(d\sigma)_{max+}$ [$\times 10^4$ a.u.]	R_{max+} [Å]	$y(d\sigma)_{max+}$ [−]
$Mo(I)_2$	4.76	5.23	3.9	0.788
$Mo(I)_2(CO)_2$	144	139	3.5	0.761

are expected to increase in the complex owing to the electron donation of the CO ligands to the central open-shell singlet Mo–Mo system, i.e., electron donation of $\Delta q = 0.602$ a.u. from both-end CO to Mo–Mo system obtained by the Hirshfeld population analysis [34] at the UCCSD level of approximation. Furthermore, such enhancement of γ_{max+} in $Mo(I)_2(CO)_2$ evokes the design guideline for enhancing γ in closed-shell donor(D)-π-donor(D) systems [35,36], which display a similar pattern, except for the central part, i.e., dσ–dσ diradical in $Mo(I)_2$. The systematic investigation of structure–property relationships in such symmetric open-shell singlet systems upon donor/acceptor substitution constitutes therefore an interesting perspective for open-shell NLO systems.

Finally, the γ density distributions are plotted for $Mo(I)_2$ and $Mo(I)_2(CO)_2$ at their R_{max} (Figure 7). For $Mo(I)_2$, the dominant contribution to γ comes from the metal–metal dσ bond region, where dominant positive and negative γ density distributions with similar shapes to those of dσ orbitals are well separated on the left- and right-hand sides (Figure 7a). For $Mo(I)_2(CO)_2$ (Figure 7b) the primary contribution to γ originates also from the metal–metal dσ bond region, where the γ density amplitudes around the out-of-phase ring components (Figure 4) are significantly enlarged as compared to those of the ligand region and of the bare system. These give rise to the large positive contributions to γ, despite the smaller inner γ density amplitudes with negative γ contributions. These results demonstrate that the significant enhancement of γ in $Mo(I)_2(CO)_2$ originates from the enhancement of the out-of-phase ring components in the metal–metal dσ bond with intermediate diradical character, caused by the axial ligand coordination. On the other hand, for $Mo(I)_2(CO)_2$ at $R_{max-} = 3.0$ Å, the γ density distribution (Figure 7e), which gives a negative contribution to γ_{max-}, presents a similar pattern to that of α density distribution at $R = 3.2$ Å (Figure 7f). This feature also substantiates the fact that γ_{max-} is dominated by type II, which is proportional to α^2 [Eq. (6), or the third power]. Moreover, around $R = 3.3$ Å, where γ is close to zero, the γ density distribution (Figure 7d) does not disappear but undergoes significant cancellation between its positive and negative contributions, which are caused by the mixing of type II (see for example, Figure 7e) and III-2 (see for example, Figure 7b) γ density distributions. Such mixing of γ density distributions of type II and III-2 is more clearly observed for $R = 3.4$ Å (Figure 7c).

4. Concluding remarks

The axial ligand effects on the diradical characters (y) and the longitudinal second hyperpolarizabilities (γ) of transition-metal dinuclear model systems have been investigated at the UCCSD level. For $y \sim 0.8$, which is primarily caused by the dσ electron contributions, both $Mo(I)_2$ and $Mo(I)_2(CO)_2$ systems show similar diradical character dependence of γ, i.e., a significant enhancement of positive γ. This result demonstrates that metal–metal multiply bonded complexes with axial ligands belong to the 'σ-dominant' third-order NLO systems similar to the open-shell singlet bare transition-metal bonded systems. The axial ligand effect on $y(d\sigma)$, which is increased as compared to that of the bare system with the same metal–metal bond length (R), originates from the shrinking of bond-axis components of the dσ orbitals, which weakens the d–d bonding interaction, due to the out-of-phase

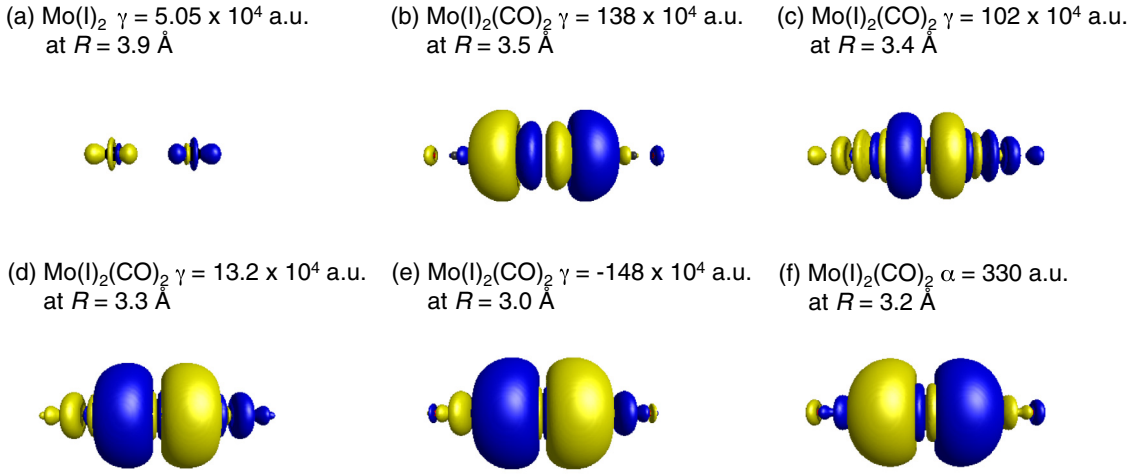

Figure 7. Total γ density distribution for $Mo(I)_2$ (a) and $Mo(I)_2(CO)_2$ (b) at R_{max} [=3.9 Å for $Mo(I)_2$ and 3.5 Å for $Mo(I)_2(CO)_2$] calculated using the UCCSD method. Total γ density distributions of $Mo(I)_2(CO)_2$ at $R = 3.4$ Å (c), $R = 3.3$ Å (d) and $R_{max-} = 3.0$ Å (e) are also shown together with total α density distribution at $R = 3.2$ Å (f). The yellow and blue surfaces represent the positive and negative γ (α) densities with contour values of ±1000 a.u. (±0.025 a.u.).

sd_{z^2} hybridization caused by axial ligand coordination. In addition to the positive maximum γ value at R_{max+}, $Mo(I)_2(CO)_2$ is found to present a negative extremum γ value at R_{max-} smaller than R_{max+}, the feature of which is predicted to be caused by the type II virtual excitation contribution. Indeed, this negative γ values in relatively small y region are predicted to appear in the case of a finite $2K/U$ region, where K is the direct exchange integral in the LNO representation [6]. Furthermore, it is found that although the axial ligand effects lead to the shortening of the bond length giving intermediate y values similar to the y_{max+} value of $Mo(I)_2$, γ_{max+} is about 30 times enhanced as compared to $Mo(I)_2$. Such significant enhancement is probably attributed to the decrease of the effective Coulomb repulsion by the axial ligand coordination. Highly electron-correlated *ab initio* MO calculations will be necessary for verifying this speculation. This is in progress in our laboratory.

Acknowledgments

This work is supported by a Grant-in-Aid for Scientific Research (A) (No. 25248007), a Grant-in-Aid for Bilateral Programs Joint Research Projects (JSPS – F.R.S.-FNRS), and a Grant-in-Aid for Scientific Research on Innovative Areas 'Stimuli-responsive Chemical Species' (No. A24109002a), MEXT, the Strategic Programs for Innovative Research (SPIRE), MEXT, and the Computational Materials Science Initiative (CMSI), Japan. Theoretical calculations are partly performed using Research Center for Computational Science, Okazaki, Japan. This is also supported by the Academy Louvain (ARC 'Extended π-Conjugated Molecular Tinkertoys for Optoelectronics, and Spintronics') and by the Belgian Government (IUAP N° P07-12 'Functional Supramolecular Systems').

Appendix A. Supplementary data

Supplementary data associated with this article can be found, in the online version, at http://dx.doi.org/10.1016/j.cplett.2014.05.064.

References

[1] C. Lambert, Angew. Chem., Int. Ed. 50 (2011) 1756.
[2] M. Abe, Chem. Rev. 113 (2013) 7011.
[3] Z. Sun et al., Chem. Soc. Rev. 41 (2012) 7857.
[4] T. Enoki, T. Ando, Physics and Chemistry of Graphene: Graphene to Nanographene, Pan Stanford Publishing, Singapore, 2013.
[5] M. Nakano et al., J. Phys. Chem. A 109 (2005) 885.
[6] M. Nakano et al., Phys. Rev. Lett. 99 (2007) 033001.
[7] K. Kamada et al., Angew. Chem., Int. Ed. 46 (2007) 3544.
[8] K. Kamada et al., J. Am. Chem. Soc. 135 (2013) 232.
[9] H. Kishida et al., Thin Solid films 519 (2010) 1028.
[10] K. Takauji et al., J. Phys. Chem. C 118 (2014) 4303.
[11] H. Matsui et al., Chem. Phys. Lett. 585 (2013) 112.
[12] K. Okuno et al., J. Phys. Chem. Lett. 4 (2013) 2418.
[13] H. Fukui et al., J. Phys. Chem. Lett. 2 (2011) 2063.
[14] T. Yamada et al., Chem. Phys. Lett. 579 (2013) 73.
[15] H. Fukui et al., J. Phys. Chem. A 116 (2012) 5501.
[16] S. Di Bella, Chem. Soc. Rev. 30 (2001) 355.
[17] Y. Zhang, B. Champagne, J. Phys. Chem. C 117 (2013) 1833.
[18] B. Coe, A. Avramopoulos, M.G. Papadopoulos, K. Pierloot, S. Vancoillie, H. Reis, Chem. Eur. J. 19 (2013) 15955.
[19] F.A. Cotton, C.A. Murillo, R.A. Walton, Multiple Bonds Between Metal Atoms, 3rd ed., Springer, New York, 2005.
[20] Y. Inoue et al., Chem. Phys. Lett. 570 (2013) 75.
[21] D. Andrae et al., Theor. Chim. Acta 77 (1990) 123.
[22] A.W. Ehlers et al., Chem. Phys. Lett. 208 (1993) 111.
[23] G. Maroulis, J. Phys. Chem. A. 107 (2003) 6495.
[24] B. Champagne et al., J. Chem. Phys. 122 (2005) 114315.
[25] R. Kishi et al., J. Chem. Theory Comput. 3 (2007) 1699.
[26] K. Yamaguchi, Chem. Phys. Lett. 33 (1975) 330.
[27] H.D. Cohen, C.C.J. Roothaan, J. Chem. Phys. 43 (1965) S34.
[28] A. Willetts et al., J. Chem. Phys. 97 (1992) 7590.
[29] M. Nakano et al., J. Chem. Phys. 103 (1995) 4175.
[30] M. Nakano et al., Theor. Chem. Acc. 130 (2011) 711; erratum 130 (2011) 725.
[31] M. J. Frisch, G. W. Trucks et al. GAUSSIAN 09, revision A.1; Gaussian, Inc.; Wallingford, CT, 2009.
[32] C.W. Bauschlicher Jr., J. Chem. Phys. 84 (1986) 260.
[33] M. Nakano et al., Chem. Phys. Lett. 206 (1993) 285.
[34] F.L. Hirshfeld, Theoret. Chim. Acta 44 (1977) 129.
[35] S. Hahn et al., J. Phys. Chem. A 103 (1999) 8221.
[36] M. Albota et al., Science 281 (1998) 1653.